JOURNAL OF VIROLOGY, Apr. 1992, p. 2135–2142
0022-538X/92/042135-08$02.00/0

Vol. 66, No. 4

Three-Dimensional Structure of Single-Shelled Bluetongue Virus

B. V. VENKATARAM PRASAD,[1]* S. YAMAGUCHI,[2] AND P. ROY[2,3]

Keck Center for Computational Biology, Verna and Marrs McLean Department of Biochemistry, Baylor College of Medicine, One Baylor Plaza, Houston, Texas 77030[1]; Environmental Health Sciences Department, University of Alabama at Birmingham, Birmingham, Alabama 35294[2]; and NERC Institute of Virology, Mansfield Road, Oxford OX1 3SR, United Kingdom[3]

Received 23 September 1991/Accepted 19 December 1991

The three-dimensional structure of single-shelled bluetongue virus has been determined to a resolution of 3 nm by using electron cryomicroscopy and image-processing techniques. The single-shelled virion has a diameter of 69 nm. The three-dimensional structure of the virion has icosahedral symmetry with a triangulation number of 13 in a left-handed configuration. The three-dimensional structure can be described in terms of two concentric layers of density surrounding a central core density. Two distinctive features of the outer layer are the 260 knobby capsomeres located at all the local and strict threefold axes and the aqueous channels located at all the five- and six-coordinated positions. These protrusions extend outward from an inner radius of 28 nm. They are interconnected out to a radius of 30 nm by saddle-shaped densities across the local and strict twofold axes. The aqueous channels surrounded by these capsomeres are about 8 nm wide at the outer surface and 8 nm deep. Some of these channels extend inward, penetrating the inner layer. These channels may provide pathways for transporting the metabolites and mRNA during the transcriptase activity of the particles. The inner layer is a featureless smooth bed of density except for the indentations in register with the channels of the outer layer. We propose that the 260 capsomeres in the outer layer are made up of trimers of the major protein, VP7, and that the inner layer is composed of the second major protein, VP3. The density in the central portion of the structure at a radius of less than 21 nm is likely due to the minor proteins and the genomic RNA.

Bluetongue virus (BTV) is the prototype member of the *Orbivirus* genus in the *Reoviridae* family (11). It causes disease primarily in sheep but can also infect cattle and goats. It is transmitted by and replicates in insects. BTV infections account for significant economic losses in the domestic livestock industry (21). A related virus causes the human disease Colorado tick fever (9, 38). Like other members in the *Reoviridae* family, BTV is a double-shelled virus with multiple double-stranded RNA segments. The outer shell is composed of two major proteins, VP5 and VP2. The single-shelled particle enclosed within this shell is composed of two major proteins, VP7 and VP3, and three minor proteins, VP1, VP4, and VP6 (25, 26, 40, 41, 43). The number of copies of these polypeptides per virion has yet not been worked out. In addition to the seven structural proteins, the genomic RNA codes for three nonstructural proteins (15, 36). The outer shell of BTV, unlike those of the reoviruses and rotaviruses, is fuzzy and very loosely bound to the inner-shell proteins. The outer shell is easily removed during purification procedures. The single-shelled particles resulting from the removal of the outer shell exhibit RNA-dependent RNA polymerase activity (40, 42).

Orbiviruses, particularly BTV, have been subjected to several structural studies by using conventional electron microscopy techniques (8, 29, 30, 39, 41). Although these studies all agree on the icosahedral symmetry of the single-shelled particles, there is disagreement on the triangulation (T) number of the icosahedron. We have used electron cryomicroscopy and computer image reconstruction methods to determine the three-dimensional structure of the single-shelled BTV particles to a resolution of 3 nm. In recent years this technique has been very useful in providing three-dimensional structural information on several large icosahedral viruses (2, 3, 14, 32, 35, 37, 45, 46). We initiated these studies to establish structure-function relationships in orbiviruses and to look for common architectural principles among the members of the *Reoviridae*. It should be mentioned here that BTV particles without the outer shell, i.e., single-shelled particles, also are called cores in the literature. We have opted to refer to these particles as single-shelled particles so as to be consistent with the literature on rotaviruses (10, 19).

MATERIALS AND METHODS

Virus and cells. United States prototype BTV type 10 (CA-10) was plaque cloned, using monolayers of BHK-21 cells. The mature virus and the single-shelled particles (cores) were obtained essentially as described by Mertens et al. (27). BHK-21 cells (1.5×10^9) were infected at a multiplicity of 5 PFU per cell and incubated at 35°C. The cells were harvested after 48 h of infection, pelleted, and homogenized in TNET buffer (50 mM Tris-HCl [pH 8.0], 0.2 M NaCl, 5 mM EDTA, 0.5% Triton X-100). The nuclei were separated as described by Mertens et al. (27). The virus particles were then recovered from cytoplasmic extracts by centrifugation on a discontinuous sucrose gradient (40 to 66% [vol/wt]). The virus band was collected and treated with chymotrypsin (40 μg/ml), followed by sodium lauryl sulfate treatment (final concentration, 1%). The released single-shelled particles then were purified through a discontinuous CsCl gradient (34 to 44%), followed by dialysis in 0.01 M Tris-HCl (pH 8.0) buffer.

Electron cryomicroscopy. A 4-μl aliquot of the virus suspension was applied to electron microscopy grids coated with holey carbon film. After blotting off the excess sample, the grid was plunged into liquid ethane by using a mechanical

* Corresponding author.

guillotine device (1, 7) inside a biohazard containment box (18). The frozen specimen was transferred under liquid nitrogen to a Gatan cryospecimen holder. The specimen was then examined in a JEOL1200 electron microscope operated at −153°C. Images were recorded with electron doses of 400 to 600 electrons per nm^2 at a nominal magnification of 30,000×.

Image processing. An electron micrograph with a good number of particles (~70) and without any visible drift was chosen for computer image processing. The micrograph was digitized on a Perkin-Elmer 1010M scanning densitometer at a step (pixel) size of 25 μm by 25 μm, which corresponds to 0.83 nm by 0.83 nm per pixel in the object. The individual virus particles selected for processing were boxed into 128 by 128 pixel areas, masked from the surroundings with a circular mask of suitable radius, and floated in a uniform background. The image-processing scheme was essentially similar to that used in previous reconstructions of other virus structures by electron cryomicroscopy (2, 14, 32, 35). All of the calculations were done on a MicroVAX 3600. The orientations of the particles were determined by the "common lines" procedure developed by Crowther (5, 6). In addition, statistical analysis similar to that used by Fuller (14) was also included in the orientation search. Once the orientations of the particles were determined, their phase origins were refined. The refinement of the origin and the orientation were carried out iteratively until no further changes occurred. The orientation of each particle was then refined with respect to the entire data set, using cross-common lines (14). The changes in the orientations of the particles after this refinement were within plus or minus 1 degree, and the phase residuals of the particles were consistently lowered by an average of a degree. The three-dimensional structure was reconstructed from the images by using cylindrical expansion methods (5, 6). The underfocus value of the electron micrograph (~1.5 μm) permitted reconstruction of the structure to 3-nm resolution with no correction for the phase reversal owing to the contrast transfer function of the electron microscope. The three-dimensional electron density map was projected along the orientations of the individual particles that were used in the reconstruction to ensure the reliability of the reconstruction. These projected density maps were cross-correlated with their respective images to more accurately locate the particle centers. This process was followed by another refinement cycle of the orientation parameters. The final reconstruction was carried out using 33 particles with unique orientations selected from 60 particles that were digitized and processed.

Radial-density plots. Radial-density plots were obtained as described by Vigers et al. (44) (see also reference 31). The radial-density functions were computed from the final three-dimensional maps by averaging densities in concentric shells of 0.833-nm width about the center of the map. The results were plotted as average density per shell against the equatorial radius of that shell. Only those density values which were above a certain cutoff value were used in the averaging. The values in a three-dimensional electron-density map correspond to contributions from both solvent (ice) and the protein mass. Because of the noticeable contrast that exists between the virion surface and ice it is not difficult to estimate the density value, i.e., the cutoff value, which best signifies the solvent-protein boundary. The density above such a cutoff value was considered to represent the protein mass. The total protein mass in the various shells of the capsid was calculated from the volume determined from the three-dimensional map, assuming a density of 1.30 g/cm^3. A very similar radial-density distribution (with respect to positions of peaks and valleys) was obtained by using a reconstruction from the particles in a micrograph recorded at higher underfocus (3 μm) and also from another independent reconstruction, using another micrograph with the same underfocus. The errors due to Fourier termination and the contrast transfer function on the radial-density distribution were therefore judged to be minimal.

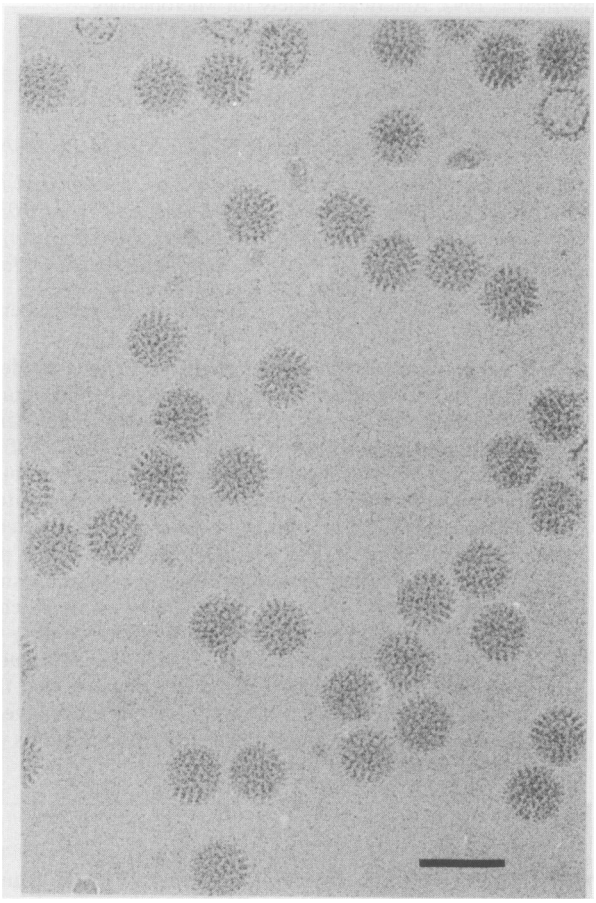

FIG. 1. Electron micrograph of single-shelled BTV particles embedded in a thin layer of vitreous ice. Bar, 100 nm.

Handedness of the icosahedral lattice. The handedness of the structure was determined by analyzing the corresponding images of the virus particles in ice from a tilt pair by a method similar to that described by Klug and Finch (20). The details of the procedure will be published elsewhere (34). As a control we used exactly the same procedure to determine the handedness of the rotavirus SA11 (clone 3) and found it to be left-handed. Rotavirus has been determined by other methods to be left-handed in several laboratories (24, 28, 35). Extreme care was taken at all stages, during electron cryomicroscopy, digitization, computer image processing, and visualization with computer graphics, for any possible hand flipping.

RESULTS

Electron cryomicroscopy. Figure 1 shows an electron micrograph of single-shelled BTV particles embedded in a thin layer of vitreous ice. The particles are spherical, with a diameter of 69 nm. Small protrusions seen around the

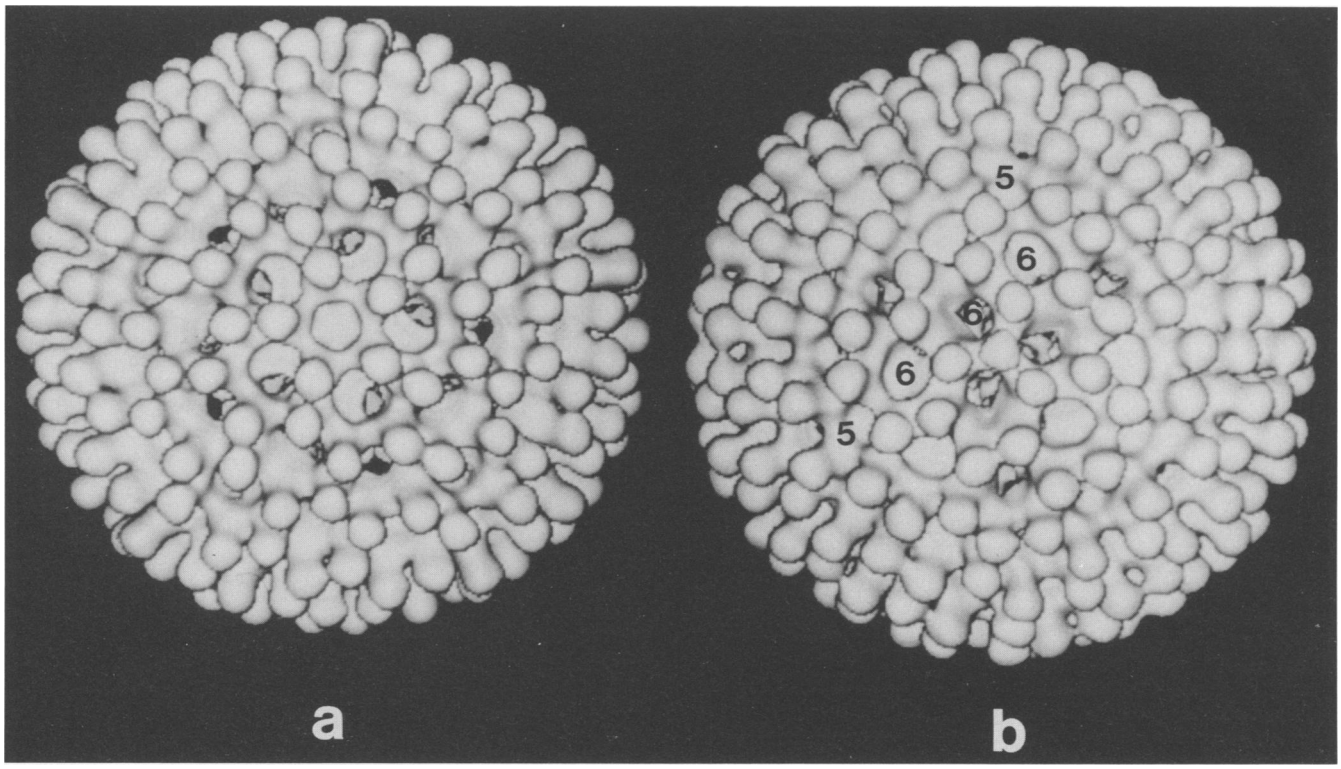

FIG. 2. Surface-shaded representations of the three-dimensional structure of the single-shelled BTV virion, viewed along the icosahedral five- (a) and threefold (b) axes. In panel b, a pair of neighboring fivefold axes (designated as 5) and the six-coordinated positions (designated as 6) relating them are shown to illustrate T=13*l* *(laevo)* (also see Fig. 4).

perimeter of these particles give them a bristly appearance. The images look very similar to those of single-shelled rotavirus particles (35). Occasionally we also see some empty single-shelled particles. In these images, the protein mass appears darker because of the higher scattering density of protein compared with that of ice. The three-dimensional structure has been determined by combining various views of the particles obtained from such a micrograph.

Three-dimensional reconstruction. Figure 2 shows surface-shaded representations of the three-dimensional structure along the icosahedral five- and threefold axes. The three-dimensional structure was reconstructed by using 33 particles with unique orientations. These particles quite adequately sample the asymmetric unit of the icosahedron. The orientation of the particles chosen for the final reconstruction is shown in Fig. 3. The average phase residual for these particles, including all the data up to a resolution of 3 nm, is about 38°; between 3.5 and 3 nm, the phase residual is about 75°; and at a resolution higher than 3 nm, the phase residual is about 90° or higher.

The virus structure shows icosahedral symmetry (Fig. 2). In the three-dimensional reconstruction, a lower 522 symmetry is used instead of the complete 532 (icosahedral) symmetry. The icosahedral symmetry is confirmed by the presence of excellent threefold symmetry is the reconstruction. The overall "R-factor" (as defined in reference 37) between the threefold enforced and threefold unenforced reconstructions was 8%. The presence of a good threefold symmetry not only confirms the icosahedral symmetry but also indicates the reliability of the reconstruction. A further check on the reliability of the reconstruction was made by comparing the real images of the particles with the two-dimensional projections obtained from the reconstructed three-dimensional map in the corresponding orientations.

An icosahedron is characterized by a triangulation (T) number which designates the relationship between the neighboring fivefold axes (4). The surface features of the three-dimensional structure of the BTV core, unambiguously shows that the T number is 13. A T=13 icosahedral lattice is a skewed lattice with handedness. In such a lattice, a fivefold axis is reached from its neighboring fivefold axis by stepping over three six-coordinated positions and taking either a left or a right turn. From the three-dimensional structure analysis, it is not possible to determine the absolute handedness. Absolute handedness has to be determined by examining "one-sided" images, using a metal-shadowing technique, or by tilting experiments. Our analysis of the electron micrographs of the virus particles in a tilt pair has shown that single-shelled BTV has a left-handed lattice (Fig. 2b and 4). It is interesting to note that other viruses in the family of *Reoviridae*, such as rotaviruses and reoviruses, also have T=13 icosahedral lattices in a left-handed configuration (24, 28, 35).

Radial-density plot. One of the advantages of electron cryomicroscopy is that it provides not only the surface details of the molecular assembly but also provides structural information at lower radii. This is in contrast to image reconstruction of a negatively stained specimen which is most often restricted to definition of the surface features. Figure 5 shows the radial-density plot of the three-dimensional structure of a single-shelled BTV virion. The radial-density profile provides a guideline to describe the structure at various radii. The density extends out to a radius of 34.5 nm. There are two distinct peaks, one at a radius of 27.5 nm

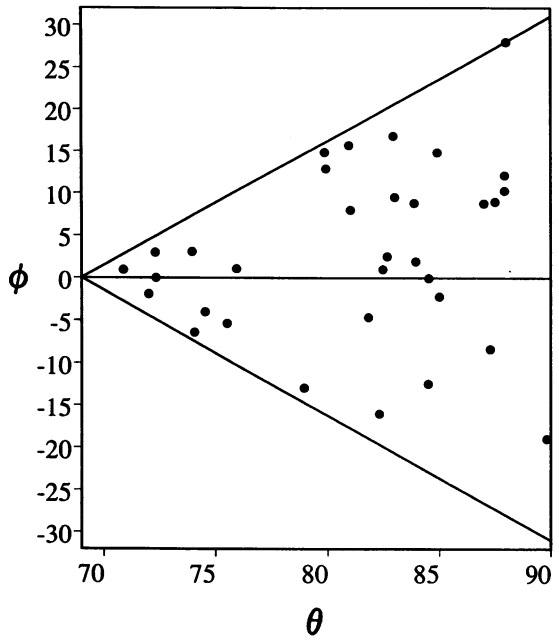

FIG. 3. Refined orientation parameters, θ and φ, of the 33 particles used in the three-dimensional structure determination. The θ and φ are defined as in reference 20. The triangle represents the icosahedral asymmetric unit.

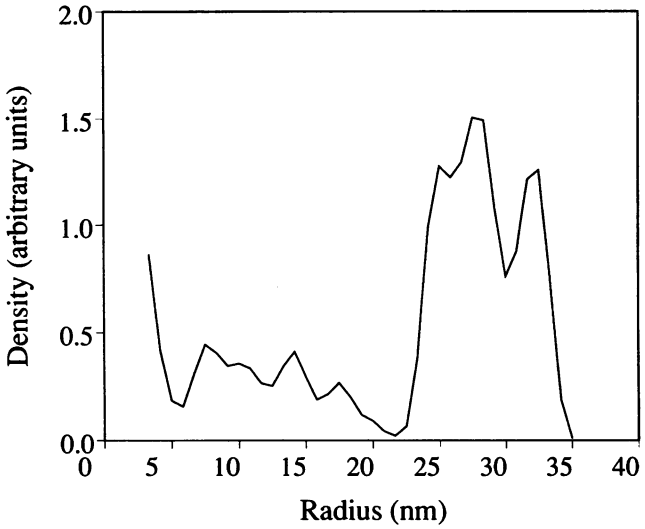

FIG. 5. Radial-density profile calculated from the three-dimensional density map. Peaks at radii of 32.5 nm and 27.5 nm correspond, respectively, to outer and inner layers.

and the other at a radius of 32.5 nm. The density decreases significantly at a radius of 21.5 nm and increases again at lower radii. The averaged radial density closer to the center, at a radius <5 nm, is not shown. This region in the three-dimensional reconstruction is dominated by noise artifacts generated on account of the Fourier-Bessel procedures used. On the basis of the radial-density profile, the three-dimensional structure may be described in terms of two concentric layers of density surrounding the internal mass referred to here as the subcore.

Knobby capsomeres. The predominant feature of the outer layer of the single-shelled particles is the presence of 260 knoblike protrusions at all the local and strict threefold axes of the T=13 icosahedral lattice. These knobs extend outward from an inner radius of 28 nm. From this radius out to a radius of 30 nm they are interconnected by densities across the local and strict twofold axes, forming saddlelike features (Fig. 2 and 6a). At the periphery they have a bulbous appearance, with an average diameter of about 4.5 nm.

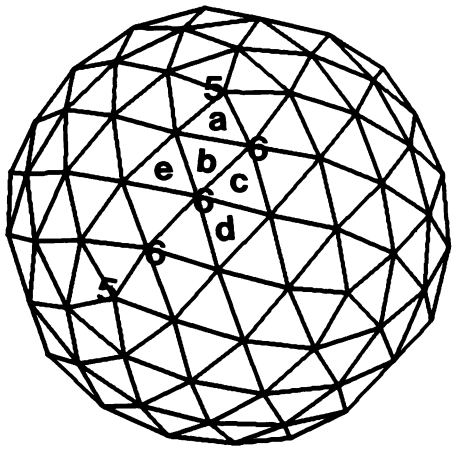

FIG. 4. A line drawing of a T=13*l* lattice. In relation to the three-dimensional structure, the center of each triangle represents the location of each knobby capsomere. a, b, c, d, and e: positions of the five types of capsomeres, classified according to their positions in the lattice. The locations of the rest of the 260 capsomeres are related to these by 532 symmetry operations.

The 260 capsomeres, on the basis of their locations in the three-dimensional structure of the single-shelled particle, can be classified into five types. These are designated as a, b, c, d, and e. The locations of one set of capsomeres are indicated in Fig. 4. The remainder of the capsomeres are related to these five by 532 symmetry operations. The intercapsomeric distances vary among the five types of capsomeres. While capsomeres a and b and c and d are respectively closer to one another, with an average distance of 5.5 nm, capsomeres b and e and b and c are farther apart, with an average distance of 6.4 nm. This introduces the asymmetry that is observed around the six-coordinated positions. Capsomere e and its twofold-related partner across the icosahedral twofold axis interact rather closely, with an intercapsomeric distance of 5.1 nm.

Aqueous channels. The capsomeres in the three-dimensional structure are arranged in such a way that there are large holes or channels at all the five- and six-coordinated positions. In accordance with the T=13 icosahedral lattice, there are 132 channels in the structure, of which 120 are along the six-coordinated positions and 12 are along fivefold axes. These channels can be categorized into three types depending on location, as in the case of rotavirus structure (35). Type I channels are those along the icosahedral fivefold axes, type II channels are those surrounding the fivefold axes, and type III channels are those around the icosahedral threefold axes. These channels are about 8 nm wide at the outer surface, decreasing to a width of about 5 nm at the point at which they meet the inner layer (Fig. 6a and b).

Inner layer. The mass density around the second peak in the radial-density plot, between a radius of 21.5 and 28 nm, makes a smooth bed upon which the capsomeres are located.

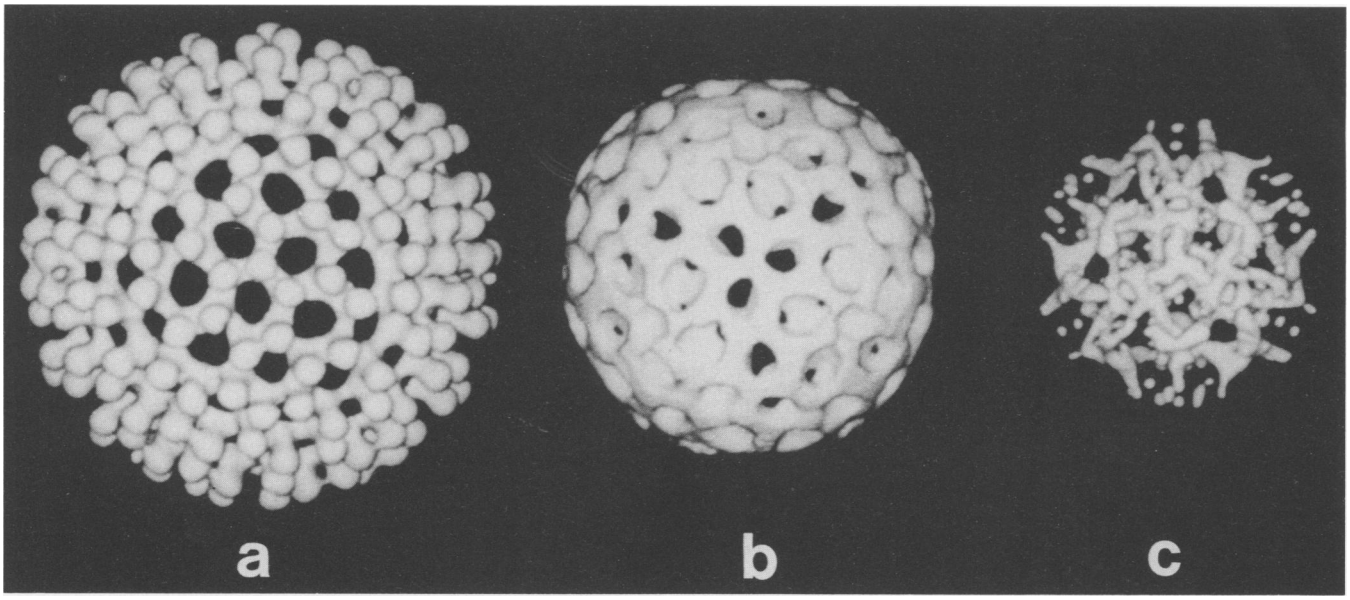

FIG. 6. Surface-shaded representations of the density in the outer layer (a), inner layer (b), and the subcore (c) as viewed along the icosahedral threefold axis. Only the upper hemisphere is displayed for clarity.

The surface of this layer is featureless but for the indentations radially in register with the channels of the outer layer (Fig. 6b). The type I channels, i.e., those at the five-coordinated positions, terminate inside the inner layer at a radius of 25 nm, forming a small indentation. The type II channels also appear to terminate at this radius. However, the type III channels traverse this layer into the subcore. The indentations at the six-coordinated positions are considerably larger than those at the fivefold axes.

DISCUSSION

Biochemical studies from several laboratories have inferred that the single-shelled particles are composed of two major proteins, VP7 (38 kDa) and VP3 (103 kDa), and the minor proteins VP1 (150 kDa), VP4 (77 kDa), and VP6 (38 kDa) (13, 25, 26, 40, 41). Sodium dodecyl sulfate gel analysis of the viral proteins clearly indicates that VP7 is present in significantly larger quantities than VP3. The immunogold-labelling studies of Hyatt and Eaton (17) on the BTV single-shelled particles strongly suggest that VP7 is located at the surface of the single-shelled particle. In the three-dimensional structure, the prominent surface features are the knobby capsomeres. Assigning the major protein VP7 to the capsomeres is therefore quite consistent with biochemical and immunogold-labelling studies. The shape and location of these capsomeres on the local and strict threefold axes strongly suggest trimeric aggregation. At the periphery, the capsomeres are not so obviously triangular. However, when the individual sections in the three-dimensional map are examined, the triangular shape is quite evident (Fig. 7). From a radius of about 29 to 32 nm the capsomeres show a triangular shape and beyond this radius they have a pronounced bulbous shape. Since there are 260 capsomeres, each virion would then have 780 molecules of VP7. The solvent-excluded volume between the radii of 28 and 34.5 nm is 3.8×10^4 nm^3. Assuming a protein density of 1.30 g/cm^3, the mass calculated from this volume is in excellent agreement, with 780 molecules of VP7.

Figure 6a and b shows the three-dimensional structural features in the outer and the inner layers, respectively. It appears that the inner layer provides a base or a scaffold on which the knobby capsomeres of the outer layer are assembled. Apart from VP7, VP3 is the more predominant protein of the single-shelled particle. Several lines of evidence indicate that VP3 is located in the inner layer. One strong piece of evidence comes from the recent studies of VP7 and VP3 expressed in baculovirus. The recombinant baculovirus particles expressing both VP7 and VP3 genes form particles which resemble empty single-shelled particles (12). The thickness of the shell formed by VP7 and VP3 in these reconstituted particles as measured from electron cryomicrographs (data not shown) is in excellent agreement with the combined thickness of the outer and the inner shells in our reconstruction. Figure 8 shows an electron cryomicrograph of the naturally occurring, empty, single-shelled particles which very much resemble the reconstituted particles. The dark ring attributable to the inner layer density is clearly evident. The radius of the empty region inside the dark ring in these particles measures 21.5 nm. Although these observations clearly indicate that VP7 and VP3 are located at a radial distance between 21.5 and 34.5 nm, they do not point out the locations of these proteins.

When expressed independently of VP3 in baculovirus, VP7 does not form icosahedral structures (12). It is therefore likely that VP7 requires close interaction with VP3. Louden and Roy (23) have demonstrated that disruption of the reconstituted particles (of VP7 and VP3) by continued dialysis yielded smooth ringlike structures containing only VP3. The diameter of these structures is consistent with the diameter of the inner layer. The assignment of VP3 to the inner layer is consistent with these experiments. Thus we can infer that VP3 and VP7 molecules closely interact at a radius of about 29 nm, which is the interface between the inner and outer layers. In this context it is noteworthy that none of the three minor proteins nor the 10 double-stranded RNA segments are found necessary, by reconstitution experiments using baculovirus-expressed proteins, for the as-

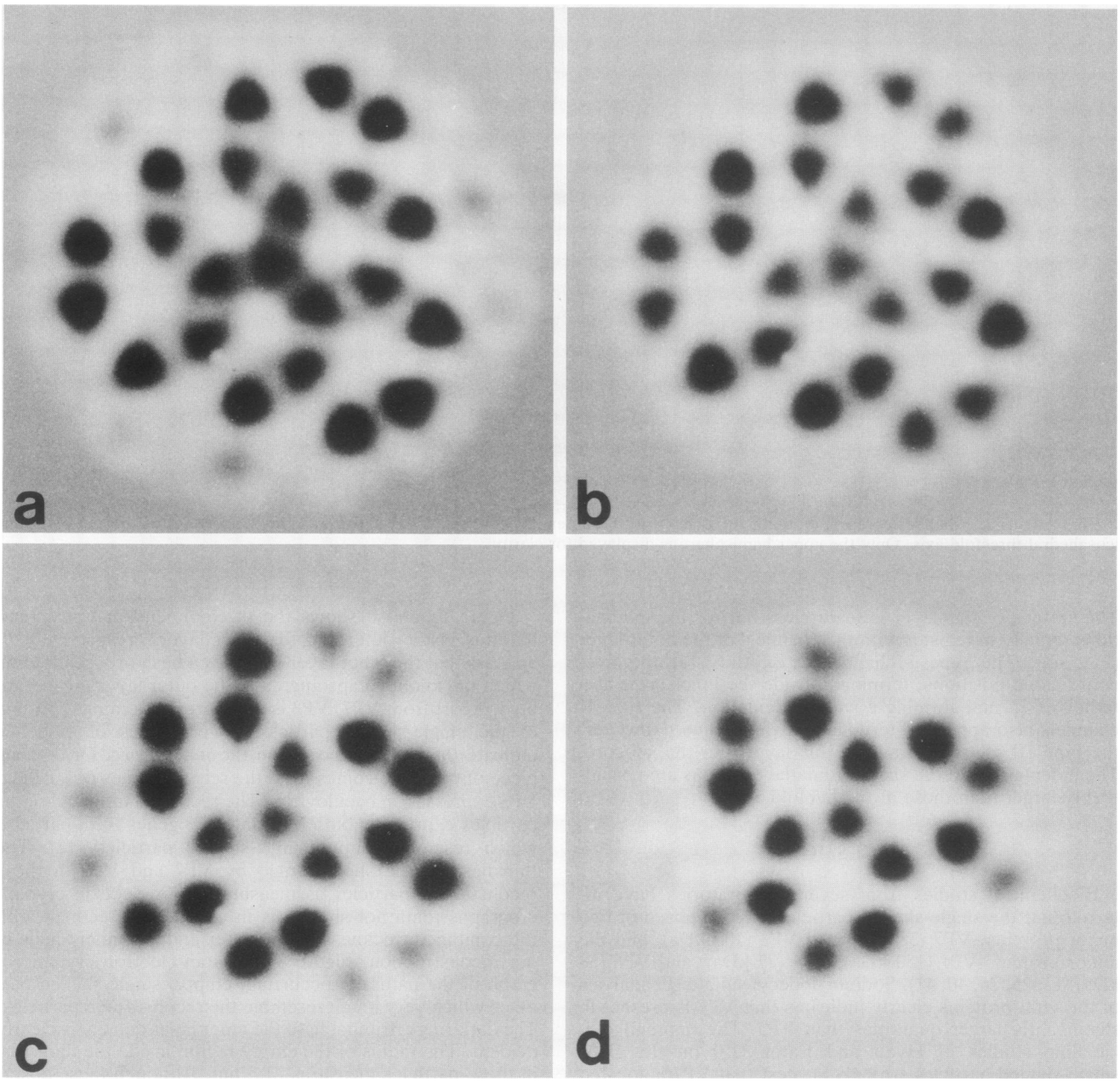

FIG. 7. Sections taken from the three-dimensional density map perpendicular to the icosahedral threefold axis at radii 29.2 (a), 30.0 (b), 30.8 (c), and 31.6 (d) nm. Note the triangular shape of the capsomeres at and immediately around the icosahedral threefold axis. The dark regions correspond to the regions of higher scattering density (i.e., proteins). Lighter regions represent the regions of lower scattering density (i.e., solvent).

sembly of empty single-shelled particles (12, 23). Thus, it is possible that the inner shell is made up predominantly of VP3. Furthermore, the interpretation that the inner layer is composed of VP3 is in good agreement with the studies of Huismans et al. (16). These authors reported that shortly after infection, parental double-shelled virions are first converted to single-shelled particles of 470S and then to smaller 390S particles. These smaller particles, which appeared skeletonlike in the electron microscope, contained only VP3 along with other minor proteins (VP1, VP4, and VP6). We think that these smaller particles are composed of the inner layer and the subcore.

At a radius of 21.5 nm, the radial density decreases but increases immediately thereafter, indicating the presence of more mass, which we have referred to as subcore. Apart from VP7 and VP3, which we have attributed to outer and inner layers, respectively, the only other proteins of the single-shelled particles are VP1, VP4, and VP6. These are the minor proteins of the single-shelled particles. In addition to these proteins, 10 segments of double-stranded RNA also would contribute to the density in this region. Figure 6c shows a surface representation of the structure at a radius of 21 nm. At this level, it is to be expected that the RNA-protein interactions would predominate within the structure.

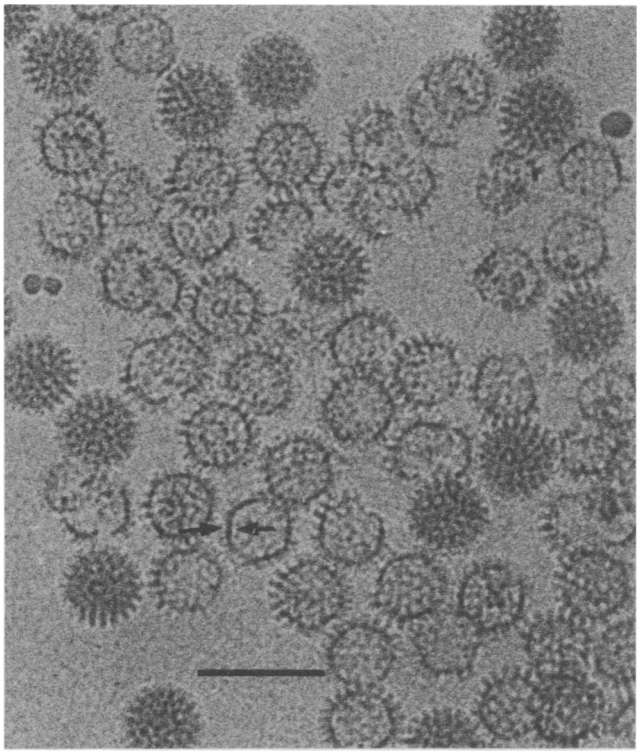

FIG. 8. Electron micrograph of the empty single-shelled BTV particles embedded in a thin layer of vitreous ice. Also seen in this micrograph are some full single-shelled particles. The dark ring corresponding to the inner layer is shown by arrows. Bar, 100 nm.

FIG. 9. Surface representation of the three-dimensional structure of the single-shelled BTV virion viewed along the icosahedral threefold axis, showing the outer and inner layers in yellow and grey, respectively. Through the channels around the icosahedral threefold axis, the density in the subcore can be seen (dark blue).

It is not known whether the structure at this radius actually conforms to the icosahedral symmetry. The exactness of the structural features at these lower radii may have to be viewed with caution because errors due to our reconstruction procedures tend to accumulate toward the center.

The three-dimensional structure of single-shelled BTV described here has similar features to those observed in the structure of single-shelled rotaviruses (35). In single-shelled rotavirus particles, trimers of VP6 protein constitute the protrusions in much the same way as VP7 in single-shelled BTV. The radial-density profiles of both these structures also are very similar (33, 46). It has been proposed that the polypeptide VP2 in rotavirus, which would be equivalent of the VP3 in BTV, forms the innermost layer upon which the trimers of VP6 are located (33). Recent experiments with baculovirus-expressed VP2 of rotavirus are in agreement with this proposal (22).

In summary, we have determined the three-dimensional structure of the single-shelled BTV to a resolution of 3 nm, using electron cryomicroscopy and computer image reconstruction procedures. The structure has icosahedral symmetry with a triangulation number of 13 in a left-handed configuration. The structure is divided into two layers of density enclosing the subcore (Fig. 9). The outer layer has 260 knoblike capsomeres made up of trimers of VP7. These protrusions are arranged in such a way that there are 132 channels at all five- and six-coordinated centers. The capsomeres of the outer layer are assembled atop the inner layer of about 70 nm thick which is proposed to be made up predominantly of VP3. These two layers enclose the subcore, which we believe is composed of the minor proteins VP1, VP5, and VP6 and the genome. The structural organization in the single-shelled BTV is similar to that in the single-shelled rotavirus (35) which also belongs to *Reoviridae*. This is not surprising, considering that these viruses have similar biochemical properties. Both single-shelled BTV and rotavirus particles exhibit transcriptase activities which can be stimulated in vitro (10, 40, 42). The structural integrity of the single-shelled particles has been shown to be necessary during transcription. The structures of rotavirus and BTV provide us with an idea as to how this process could take place. For both of these viruses it is likely that the network of aqueous channels provides pathways for the necessary metabolites to reach the transcriptional sites and for the nascent mRNA molecules to exit.

ACKNOWLEDGMENTS

We gratefully thank W. Chiu for encouragement, support, and many helpful discussions. We also thank T. S. Baker and S. D. Fuller for providing a version of the SIMPLEX computer program and G. J. Wang, Ms. R. Rothnagel, and Mr. J. R. Lalison for excellent technical help.

This work was partly supported by NIH grants AI26879 and GM41064. We gratefully acknowledge the use of the electron microscope and computing facility at the 3DEM Resource Center (supported by NIH RR02250 and the W. M. Keck Foundation).

REFERENCES

1. **Adrian, M., J. Dubochet, J. Lepault, and A. McDowell.** 1984. Cryo-electron microscopy of viruses. Nature (London) **308**:32–36.
2. **Baker, T. S., J. Drak, and M. Bina.** 1988. Three-dimensional structure of SV40. Proc. Natl. Acad. Sci. USA **85**:422–426.
3. **Baker, T. S., W. W. Newcomb, F. P. Booy, J. C. Brown, and A. C. Steven.** 1990. Three-dimensional structures of maturable and abortive capsids of equine herpesvirus 1 from cryoelectron microscopy. J. Virol. **64**:563–573.

4. **Caspar, D. L. D., and A. Klug.** 1962. Physical principles in the construction of regular viruses. Cold Spring Harbor Symp. Quant. Biol. **27**:1–32.
5. **Crowther, R. A.** 1971. Procedures for three-dimensional reconstruction of spherical viruses by Fourier synthesis from electron micrographs. Proc. R. Soc. Lond. Ser. B **261**:221–230.
6. **Crowther, R. A., D. J. DeRosier, and A. Klug.** 1970. The reconstruction of a three-dimensional structure from projections and its application to electron microscopy. Proc. R. Soc. Lond. Ser. A **317**:319–340.
7. **Dubochet, J., M. Adrian, J. J. Chang, J. C. Homo, J. Lepault, A. W. McDowall, and P. Schultz.** 1988. Cryo-electron microscopy of vitrified specimens. Q. Rev. Biophys. **21**:129–228.
8. **Els, H. J., and D. W. Verwoerd.** 1969. Morphology of bluetongue virus. Virology **38**:213–219.
9. **Emmons, R. W.** 1966. Colorado tick fever: prolonged viremia in hybernating *Citellus lateralis*. Am. J. Trop. Med. Hyg. **15**:428–433.
10. **Estes, M. K.** 1990. Rotaviruses and their replication, p. 1353–1404. *In* B. N. Fields, D. M. Knipe, R. M. Chanock, J. L. Melnick, B. Roizman, and R. E. Hope (ed.), Virology. Raven Press, New York.
11. **Fenner, F.** 1976. Classification and nomenclature of viruses, second report of the international committee on taxonomy of viruses. Intervirology **7**:1–115.
12. **French, T. J., and P. Roy.** 1990. Synthesis of bluetongue virus (BTV) corelike particles by a recombinant baculovirus expressing the two major structural proteins of BTV. J. Virol. **64**:1530–1536.
13. **Fukusho, A., Y. Yu, Y. Yamaguchi, and P. Roy.** 1989. Completion of the sequence of bluetongue virus serotype 10 by the characterization of structural proteins VP6 and a non-structural protein, NS2. J. Gen. Virol. **70**:1677–1689.
14. **Fuller, S. D.** 1987. The T=4 envelope of Sindbis virus is organized by interactions with a complimentary T=3 capsid. Cell **48**:923–934.
15. **Gorman, B. M., J. Taylor, P. J. Walker, W. L. Davidson, and F. Brown.** 1981. Comparison of bluetongue type 20 with certain viruses of the bluetongue and Eubenagee serological groups of orbiviruses. J. Gen. Virol. **57**:251–261.
16. **Huismans, H., A. A. Van Dijk, and H. J. Els.** 1987. Uncoating of parental blue-tongue virus to core and subcore particles in infected L cells. Virology **157**:180–188.
17. **Hyatt, A. D., and B. T. Eaton.** 1988. Ultrastructure and distribution of the major capsid proteins within bluetongue virus and infected cells. J. Gen. Virol. **69**:805–815.
18. **Jeng, T.-W., Y. Talmon, and W. Chiu.** 1988. Containment system for the preparation of vitrified-hydrated virus specimen. J. Electron Microsc. Technol. **8**:343–348.
19. **Kapikian, A. Z., and R. M. Chanock.** 1990. Rotaviruses, p. 1353–1404. *In* B. N. Fields, D. M. Knipe, R. M. Chanock, J. L. Melnick, B. Roizman, and R. E. Hope (ed.), Virology. Raven Press, New York.
20. **Klug, A., and J. T. Finch.** 1968. Structure of viruses of the papilloma-polyoma virus type. IV. Analysis of tilting experiments in the electron microscope. J. Mol. Biol. **31**:1–12.
21. **Knudson, D. L., and T. P. Monath.** 1990. Orbiviruses, p. 1353–1404. *In* B. N. Fields, D. M. Knipe, R. M. Chanock, J. L. Melnick, B. Roizman, and R. E. Hope (ed.), Virology. Raven Press, New York.
22. **Labbe, M., A. Charpilienne, S. E. Crawford, M. K. Estes, and J. Cohen.** 1991. Expression of rotavirus VP2 produces empty corelike particles. J. Virol. **65**:2946–2952.
23. **Loudon, P. T., and P. Roy.** 1991. Assembly of five blue-tongue virus proteins expressed by recombinant baculoviruses: inclusion of the largest protein VP1 in the core and virus-like particles. Virology **180**:798–802.
24. **Ludert, J. E., F. Gil, F. Liprandi, and J. Esparza.** 1986. The structure of rotavirus inner capsid studied by electron microscopy of chemically disrupted particles. J. Gen. Virol. **67**:1721–1725.
25. **Martin, S. A., and H. J. Zweernik.** 1972. Isolation and characterization of two types of blue-tongue virus particles. Virology **50**:495–506.
26. **Mertens, P. P. C., F. Brown, and D. V. Sangar.** 1984. Assignment of the genome segments of bluetongue virus type 1 to the proteins which they encode. Virology **135**:207–217.
27. **Mertens, P. P. C., J. N. Burroughs, and J. Anderson.** 1987. Purification and properties of virus particles, infectious subviral particles, and cores of bluetongue virus serotypes 1 and 4. Virology **157**:375–386.
28. **Metcalf, P.** 1982. The symmetry of the reovirus outer shell. J. Ultrastruct. Res. **78**:292–301.
29. **Murphy, F. A., E. C. Borden, R. E. Shope, and A. Harrison.** 1971. Physico-chemical and morphological relationships of some arthropod borne viruses to bluetongue virus—a new taxonomic group. J. Gen. Virol. **13**:273–278.
30. **Murphy, F. A., P. H. Coleman, A. K. Harrison, and G. W. Gary.** 1968. Colorado tick fever virus: an electron microscopic study. Virology **35**:28–40.
31. **Olson, N. H., T. S. Baker, J. E. Johnson, and D. A. Hendry.** 1990. The three-dimensional structure of frozen-hydrated *Nudaurelia capensis* virus. J. Struct. Biol. **105**:111–122.
32. **Prasad, B. V. V., J. W. Burns, E. Marietta, M. K. Estes, and W. Chiu.** 1990. Localization of VP4 neutralization sites in rotavirus by three-dimensional cryo-electron microscopy. Nature (London) **343**:476–478.
33. **Prasad, B. V. V., and W. Chiu.** Structure of rotavirus. Top. Immunol. Mol. Biol., in press.
34. **Prasad, B. V. V., R. Rothnagel, and W. Chiu.** Unpublished data.
35. **Prasad, B. V. V., G. J. Wang, J. P. M. Clerx, and W. Chiu.** 1988. Three-dimensional structure of rotavirus. J. Mol. Biol. **199**:269–275.
36. **Sangar, D. V., and Mertens, P. P. C.** 1983. Comparison of type I bluetongue virus protein synthesis in vivo and in vitro, p. 183–191. *In* R. W. Compans and D. H. L. Bishop (ed.), Double stranded RNA viruses. Elsevier, New York.
37. **Schrag, J. D., B. V. V. Prasad, F. J. Rixon, and W. Chiu.** 1989. Three-dimensional structure of HSV-1 nucleocapsid. Cell **56**: 651–660.
38. **Spurance, S. L., and A. Bailey.** 1973. Colorado tick fever. A review of 115 laboratory confirmed cases. Arch. Int. Med. **131**:288–293.
39. **Studdert, M. J., J. Pangborn, and B. Addison.** 1966. Bluetongue virus structure. Virology **29**:509–511.
40. **Van Dijk, A. A., and H. Huismans.** 1980. The in-vitro activation and further characterization of the blue-tongue virus-associated transcriptase. Virology **104**:347–356.
41. **Verwoerd, D. W., H. J. Els, E.-M. De Villiers, and H. Huismans.** 1972. Structure of bluetongue virus capsid. J. Virol. **10**:783–794.
42. **Verwoerd, D. W., and H. Huismans.** 1972. Studies on the in-vitro and the in-vivo transcription of the blue-tongue virus genome. Onderstepoort J. Vet. Res. **38**:185–192.
43. **Verwoerd, D. W., H. Huismans, and B. J. Erasmus.** 1979. Orbiviruses, p. 285–345. *In* H. Frankel-Conrat, and R. R. Wagner (ed.), Comprehensive virology, vol. 14. Plenum Press, New York.
44. **Vigers, G. P. A., R. A. Crowther, and B. M. F. Pearse.** 1986. Location of the 100kd-50kd accessory proteins in clathrin coats. EMBO J. **5**:2079–2085.
45. **Vogel, R. H. S., W. Provencher, C.-H. von Bonsdorff, M. Adrian, and J. Dubochet.** 1986. Envelope structure of Semiliki Forest virus reconstructed from cryo-electron micrographs. Nature (London) **320**:533–535.
46. **Yeager, M., K. A. Dryden, N. H. Olson, H. B. Greenberg, and T. S. Baker.** 1990. Three-dimensional structure of rhesus rotavirus by cryoelectron microscopy and image reconstruction. J. Cell Biol. **110**:2133–2144.